JMEPEG (2021) 30:5005–5012
https://doi.org/10.1007/s11665-021-05585-8

1059-9495/$19.00

In Vivo Study on Bone Response to 3D-Printed Constructs Designed from Microtomographic Images

Lucia Pérez-Sánchez, Misael Aaron Ortiz de la O, Patricia González-Alva, Luis Alberto Medina, David Masuoka-Ito, Marco Antonio Alvarez-Perez, and Janeth Serrano-Bello

Submitted: 15 December 2020 / Revised: 28 January 2021 / Accepted: 12 February 2021 / Published online: 5 March 2021

The design of scaffolds that could adjust and adapt greatly to bone defects is a significant challenge to bone tissue engineering. Recently, 3D printing technology emerged as a process that could precisely control the architecture and design an exact geometry of the scaffold to the site or defect where it will be implanted. Thus, this research aimed to design and synthesize individualized constructs of polylactic acid (PLA) by 3D printing using microtomographic images to fit the edge of Wistar rat calvaria's critical size defects. The 3D-printed construct using the DICOM data of microtomographic images process to STL manipulated and designed by various software showed an excellent geometry. The in vitro biocompatibility assay of the 3D printing scaffold was evaluated by WST-1, showing an excellent biological response. Moreover, the in vivo evaluation of the bone regeneration process onto the rat calvaria defect model measured by the bone mineral density (BMD) at 8, 30, 60, and 90 days via micro-CT showed that at the end of the evaluation period, the 3D construct was integrated into the edges of the bone tissue, and new tissue deposited was in the process of mineralization. These findings suggest that the 3D construct matches the calvaria defect, allowing the novo mineral tissue to form. These individualized printed scaffolds may be a promising candidate in bone tissue engineering for future regeneration strategies.

Keywords 3D-printed scaffold, additive manufacturing, bone tissue engineering, customized bone scaffold, computational design

1. Introduction

Critically sized bone defects resulting from trauma, infection, degenerative disease, tumor resection, and other conditions remain a challenge for surgeons and orthopedists (Ref 1). Currently, bone defect treatments are based on the use of grafts (autografts, xenografts, alloplastics), which serve as a support matrix, filler, or stabilizers; however, they lack a structure in both shape and porosity, coupled with the fact that the volume of regenerated tissue is insufficient due to mechanical forces (xenografts and alloplastics). Furthermore, autografts can withstand such mechanical forces, but their disadvantage is their limited availability. On the other hands, these methodological strategies are incapable of generating structures that conform and adapt more precisely to the type of bone defect (Ref 2-4). Bone tissue engineering is a multidisciplinary field that has grown at an accelerated rate because it focuses on alternative treatments that ideally eliminate the clinical problems caused by grafts, with the main objectives of regenerating and maintaining bone tissue function.

In the last decade, functional tissue engineering has expanded and encompassed mechanobiological interactions between cells and scaffolds. The former implies that cells within scaffolds interact with a complex biomechanical environment. Such physical signals can significantly influence cell growth, differentiation, and metabolism. Consequently, more information is required both from the in vivo mechanical environment and the response of cells to these signals to enhance or accelerate tissue regeneration (Ref 5). As technology has advanced, bone tissue engineering has improved scaffold manufacturing techniques, biomaterials, and, recently, mesenchymal stem cell application due to their regenerative capacity.

Several manufacturing methods for 3D scaffolds production, such as solvent casting, particle leaching, gas foaming, phase separation, and electrospinning, are used. Nonetheless, they have many limitations compared to 3D printing technology, which has emerged as a valuable tool because it can design scaffolds to match the complex geometry of a defect, improving the scaffold's interaction and the host (Ref 6, 7). Other benefits are that they allow thermoplastic polymers such as polylactic acid (PLA), an aliphatic polyester derived from renewable surfaces such as sugar from corn, potatoes, and sugar cane. In the medical field, PLA is widely used due to its biocompat-

This invited article is part of a special topical focus in the *Journal of Materials Engineering and Performance* on Additive Manufacturing. The issue was organized by Dr. William Frazier, Pilgrim Consulting, LLC; Mr. Rick Russell, NASA; Dr. Yan Lu, NIST; Dr. Brandon D. Ribic, America Makes; and Caroline Vail, NSWC Carderock.

Lucia Pérez-Sánchez, Misael Aaron Ortiz de la O, Patricia González-Alva, Marco Antonio Alvarez-Perez, and **Janeth Serrano-Bello**, Tissue Bioengineering Laboratory, Postgraduate Studies and Research Division, Faculty of Dentistry, National Autonomous University of Mexico (UNAM), 04510 Mexico, CDMX, Mexico; **Luis Alberto Medina**, Instituto de Física, Universidad Nacional Autónoma de México, 04510 Mexico, CDMX, Mexico; and Unidad de Investigación Biomédica en Cáncer INCan/UNAM, Instituto Nacional de Cancerología, 14280 Mexico, México; **David Masuoka-Ito**, Stomatology Department, Health Science Center, Autonomous University of Aguascalientes, Aguascalientes, Mexico. Contact e-mails: marcoalv@unam.mx and janserbello@fo.odonto.unam.mx.

ibility with the human body, including for applications such as medical implants, surgical sutures, and medical devices (Ref 8).

Moreover, recent in vitro and in vivo studies have shown that dental pulp-derived mesenchymal stem cells (DPSC) can efficiently differentiate into bone lineage cells due to the effect of osteoinductive factors such as bone morphogenic proteins (BMP), as well as surface markers and proteins associated with the formation of mineralized tissue (alkaline phosphates, osteocalcin, and osteopontin) (Ref 9). The use of DPSC for in vivo bone regeneration has been extensively studied based on different protocols and using different experimental models and types of scaffolds with different results. Human DPSCs (hDPSCs) are capable of inducing the generation of adult bone tissue. However, scaffold materials are often necessary to optimize the 3D structure of the formed bone tissue and improve the osteoblastic differentiation of hDPSC (Ref 10-12). Thus, the study aimed to evaluate the in vivo bone regeneration in critical size defect in Wistar calvaria rats by 3D-printed constructs designed from microtomographic images that match onto the defect calvaria model.

2. Materials and Methods

2.1 Surgical Procedure for the Critical Defect in Calvaria Wistar Rat

Critical defects (9 mm diameter) were performed in the calvaria of 18-week-old male Wistar rats weighing 250 g. The surgical procedure was performed according to what was established by the Internal Committee for the Care and Use of Laboratory Animals, of the Dentistry School, with approval number CIE/10/01/2015 and the Mexican legislation NOM-062-ZOO1999.

Briefly, the animals were tranquilized and sedated intramuscularly with ketamine (80 mg/kg) and xylazine (10 mg/kg). The surgical area was shaved, and routine antisepsis was carried out with povidone-iodine. Mepivacaine with epinephrine was applied topically, and then, a linear incision of 3 cm was made through the skin and the periosteum of the calvaria until exposing the cranial vertex. To perform the critical size defect, used a trephine with a 9 mm diameter mounted on an implant motor at 4000 rpm; the standardized size defect was delimited in the middle portion frontal bone, irrigating with a sterile phosphate buffer (PBS). Subsequently, the bone fragment was cleaved with a chisel (Hu-Friedy cat. HUCO1), taking great care not to damage the dura mater. Finally, the tissue was sutured continuously with 4-0 polyglycolic acid. A postoperative clinical follow-up was carried out, assessing a series of clinical parameters: the general condition of the animal, the appearance of the wound and the operated area, bleeding, and exudate. The rat remained in photoperiod conditions of 12 h, relative humidity 50%, and the water and food were ad libitum.

2.2 Design of the Scaffold

For the design of the scaffold, one rat with the critical size defect in the calvaria underwent an imaging study through the micro-CT unit of an Albira small animal microPET/SPECT/CT imaging system (Bruker), using settings of a 0.4 mA current, 35 kV voltage, and a total of 1000 projections over 360°. The field of view was located in the defect zone (calvaria). Image reconstruction was performed using the filtered back-projection algorithm (FBP) with Albira Reconstructor software, resulting in a 558 × 558 × 516 image matrix with voxel size 125 μm^3, for a total height of 64.5 mm, with which digital imaging and communication in medicine (DICOM) were obtained. The DICOM images were transformed into STL (standard tessellation language) format employing the InVesalius© software, a medical software that reconstructs 3D images from magnetic resonance and computed tomography. The scaffold was modeled according to the defect's shape and size using the 3D Builder© software and the internal with Slic3r© software.

2.3 Scaffold Printing

The scaffolds were printed by layer-by-layer extrusion melt deposition technique of PLA (FDA approved) filament purchased from 3D Printers Puebla® with 1.75 mm thickness. The scaffold was 3D, uniform, close-pore, shape, and size of the calvaria defect, with a square pore size of 130 μm. The overall dimensions of the scaffolds were 9 mm in diameter and 1.90 mm in thickness. The PLA filament extrudes at an optimal temperature of 210 °C from 0.2 mm nozzle with flow velocity (40-70 mm/s), rectilinear fill pattern, fill density 85%, and printing time 6 min. The scaffolds were packed in high-density polypropylene bags (Tybekc bags) and sterilized by hydrogen peroxide gas plasma in the STERRAD equipment in a cycle of 54 min at a temperature of 50 °C.

2.4 Cell Culture

Mesenchymal stem cells derived from dental pulp (DPSC) previously characterized in the Mesenchymal Stem Cells Laboratory, Oncology Research Unit, Oncology Hospital, National Medical Center, IMSS, Mexico City, Mexico (Ref 13). The DPSC cells were cultivated and expanded with Dulbecco's modified eagle's medium (DMEM) supplemented with 10% fetal bovine serum (FBS), a solution of antibiotics penicillin (100 IU/ml), streptomycin (100 μg/ml), and fungizone (0.3 μg/ml). The cultures were kept at a temperature of 37 °C, in an atmosphere of 95% air and 5% CO_2 in an environment with 100% humidity.

2.5 Viability Assay

For evaluating the biocompatibility of 3D constructs, two groups were formed, the control, which consisted of non-printed PLA, a solid smooth disk with a diameter of 9 mm and 1mm of thickness, and the experimental in 3D-printed constructs. Both groups seeded with DPSC cells at a density of 2×10^4 cells/ml, subsequently, viability tests were carried out using WST-1 assay. After 1, 3, 5, 7, 14, and 21 days of culture, cells were incubated with 0.3 mg/ml of WST-1 in a 48-well plate for 4 h. Then, absorbance was measure in an ELISA plate reader (Chromate, Awareness), where the optical density was obtained at a wavelength of 450 nm to correlate the value with the metabolic activity of living cells. The culture medium was changed every two days for fresh medium during the experiment.

2.6 Surgical Procedure to Evaluate Bone Regeneration

To evaluate the capacity of the scaffolds in bone regeneration. The animals used for the animal model were 15 male, young-adults Wistar rats, with an average weight of 250 g, which were randomly assigned to three groups (n = 5): (1)

control defect only, (2) 3D-printed PLA scaffold, and (3) 3D-printed PLA scaffold with DPSC cells. The surgical procedure was described above.

2.7 Evaluation of Implanted PLA Scaffolds by Computed Microtomography (μCT)

To evaluate the quality and quantity of newly formed bone tissue, μCT images of the animals were acquired at different periods after scaffold implantation (8, 30, 60, and 90 days) using settings of a 0.4 mA current, 35 kV voltage, and a total of 1000 projections over 360°. The field of view was located in the defect zone (calvaria). To calculate the bone mineral density (BMD), performed 2.17 mm ROIs on the microtomographic images, considering three areas of interest (native bone, scaffold, and novo tissue). The results were compared using a phantom with known mg hydroxyapatite concentrations per cubic centimeter (mgHA/cc). At the end of the established period of time, the animals were euthanized by CO_2; subsequently, an osteotomy was performed to remove the shell in the defect area.

2.8 Statistical Analysis

To analyze the scaffolds' cell viability, a Mann–Whitney U analysis was performed, and to evaluate BMD, the one-way ANOVA statistical analysis was performed, with Tukey's posthoc test. The analyzes were carried out in the statistical program IBM SPSS statistics version 23, and a value of $p < 0.05$ was considered to determine statistically significant differences.

3. Results

3.1 Design and Printing of the Scaffold

Based on the microtomographic image of the critical size defect of the Wistar rats calvaria, a three-dimensional surface was obtained, using the Builder© software, where only the area of the bone defect was cut, and it was possible to design the scaffold according to the shape, size, and edges (Fig. 1a-d).

To obtain a homogeneous surface with a pore range of 130 μm, it was important to consider the limitation of resolution of the 3D printer. To overcome such limitation, the flow velocity parameters (40-70 mm/s) and the pattern were modified from filling to rectilinear, and the density was 85% to obtain the desired pore size (Fig. 1e). It was possible to design and print the scaffold with a diameter of 9 mm and a thickness of 1.90 mm (Fig. 1f).

3.2 Cellular Response to Scaffold

The viability response of the DPSC cells in the PLA 3D-printed constructs was evaluated with the WST-1 viability assay. The results show that the control group presented less proliferative activity than the experimental group from the third day and subsequently. The non-printed scaffold (smooth surface) of the control scaffold probably did not allow good cell adhesion and viability. Similarly, a notable decrease is observed at 14 days; however, at day 21, an increase was observed. The results could imply that at 14 days of culture, the cells began to secrete extracellular matrix and decreased their proliferation. Then, on the 21 days, once the extracellular matrix was secreted, the necessary conditions were obtained for the cell population to increase. In contrast, the experimental group maintained a constant proliferative activity over the days (Fig. 2), confirming a statistically significant difference between both groups with a $p < 0.05$. Therefore, the results suggested that the 3D-printed construct's microarchitecture promoted proliferative activity and demonstrated that the scaffold is not cytotoxic for DPSC cells.

3.3 Evaluation of Bone Regeneration by Microtomographic Images

To evaluate the 3D-printed PLA scaffolds' bone regeneration capacity with and without cells, microtomographic images were analyzed at different periods: 8, 30, 60, and 90 days (Fig. 3). The results showed no evidence of regeneration in the control group (scaffold-free) and that the defect of critical size remains in the rat's calvaria.

The μCT images showed that in the 3D scaffolds groups, with or without cells, the scaffold sealed the defect's edges. The group corresponding to the 3D scaffold without any presence of cells, after 8 days of evaluation, showed hypodense areas, mainly at the edges of the defect. Then, the areas became hyperdense after 30 and 60 days. However, in the center of the defect, small areas of variable density. At 90 days, a more homogeneous density can be observed in the area of the defect, with the center showing areas in the form of islands that appear empty.

In the group of the 3D-printed scaffold with DPSC, a vaporizable density is observed in the entire defect area from 8 days, with time at 30 and 60 days, greater radiodensity is observed mainly in the borders; however, there is the presence of hypodense areas mainly in the center, at 90 days greater radiodensity is distinguished, with some empty areas.

3.4 Evaluation of Bone Mineral Density (BMD)

To evaluate the radiodense areas' characteristics, the bone mineral density (BMD) was measured in three areas of interest: edges of the defect, scaffold, and novo tissue (Fig. 4, 5). As showed in Fig. 4(a) and 5, after 8 days, the results from the BMD analysis demonstrated that the novo tissue formed in the groups where the 3D-printed PLA scaffold with and without cells, and that both groups showed similar results (40.59 and 46.48 mmHA/cc, respectively), compared to the tissue that it is located on the edge since it presents a higher BMD (76.94 and 96.21 mmHA/cc), since at 8 days, the area of the defect does not have the characteristics of mineralized tissue. It is worth mention that there was a statistically significant difference between the adjacent bone of both experimental groups with a value of $p < 0.05$.

Figure 4(b) and 5 shows that at 30 days, the BMD of the novo tissue area in both groups increased (70.24 and 73.46 mmHA/cc, respectively), with no statistical difference. Figure 4(c) and 5 shows that at 60 days, the BMD of the novo tissue in the group with the 3D-printed PLA scaffold was 88.22 mmHA/cc, and the group with the 3D scaffold with DPSC was 73.71 mmHA/cc. No statistical differences were observed between groups. It was contrasting with the zone corresponding to the native bone since both groups presented statistical differences. Figure 4(d) and 5 shows that at 90 days, the BMD of the novo tissue decreased in both groups (71.87 and 65.16 mmHA/cc) compared to the previous days. It should be noted

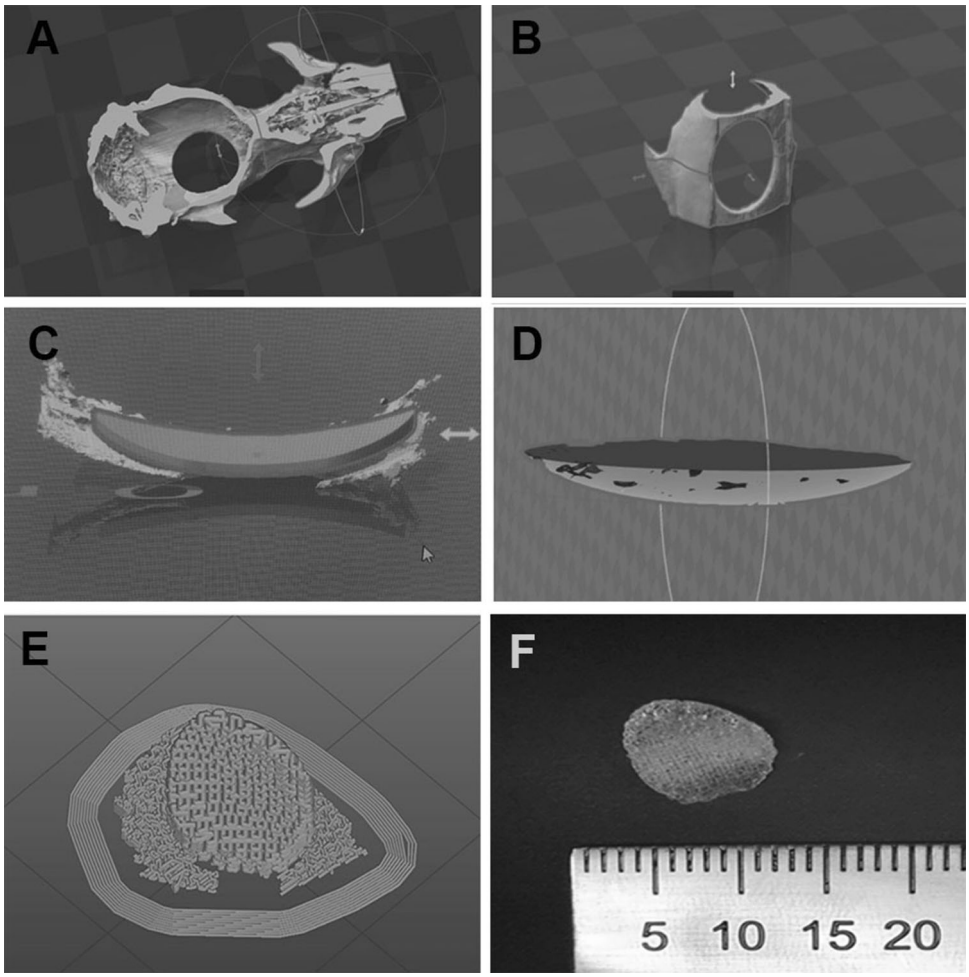

Fig. 1. Scaffold design, (a) selection of the defect area, (b) elimination of excess tissue, (c) adaptation of the scaffold to the size of the defect, respecting the concavity and convexity, (d) obtaining the scaffold, (e) rectilinear filling pattern that creates a porous surface by layer-by-layer crosslinking, additionally sacrificial material is observed, (f) 3D-printed scaffold

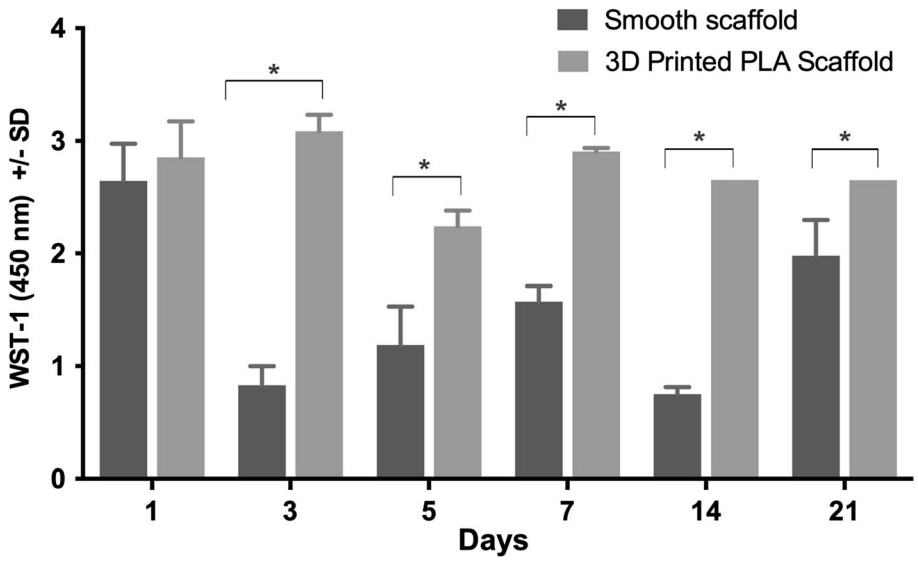

Fig. 2. WST assay showing the viability of cells evaluated at 1-21 days of mesenchymal stem cells derived from dental pulp onto the 3D-printed scaffold. Statistical significance is indicated by $*p < 0\ 05$

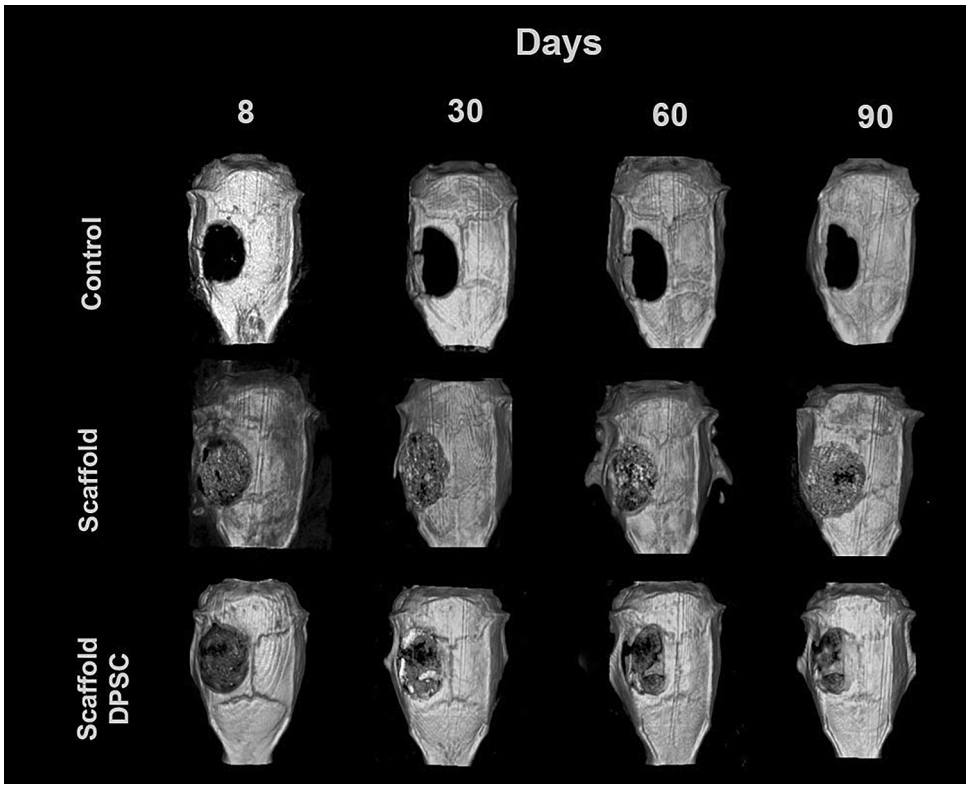

Fig. 3. Representative images of the different groups with respect to time, in the 3D-printed scaffold and scaffold DPSC group, both types of well-defined scaffolds are observed, variable radiodensity is observed throughout the defect. Hypodense areas are seen in the center of the defect in both groups

that there were no significant differences in any area of interest between the groups.

4. Discussion

Tissue engineering is a multidisciplinary field that applies the principles of engineering and life sciences to develop biological substitutes that regenerate, maintain, or improve the function of the human body's tissues (Ref 14, 15). As the field of engineering progresses, the need to create constructs with world-class biomaterials and easily accessible and reproducible manufacturing techniques have become a significant challenge. Therefore, the use of biodegradable polymers, such as PLA, has become widespread (Ref 16). PLA offers a substantial potential for its use in regenerative engineering of bone tissue, as 3D constructs, due to its mechanical properties. Its favorable degradation rate allows the design of highly interconnected porous structures, and its properties enable encapsulation growth factors, stem cells, and anti-inflammatory agents, hence, facilitating osseointegration (Ref 17).

This research commercialized PLA was used for 3D printer scaffolds with the fused deposition technique, where the DPSC cells remained viable in the PLA scaffold. It is important to mention that the scaffold sterilization process was through hydrogen peroxide plasma, where the literature reports that plasma can modify the hydrophobic surface of PLA into hydrophilic, helping cell adhesion (Ref 18, 19).

On the other hands, in the in vivo bone defect model, the rats did not show a chronic inflammatory process caused by the material, proving that PLA alone is biocompatible. The processing of PLA constructs by various techniques such as particle leaching, lyophilization, phase separation, fiber spinning, and fusion molding has disadvantages that the geometric shape and size cannot be controlled in the porous interconnectivity (Ref 16, 20).

Recently, fused deposition modeling (FDM) 3D printing technology allows precise control of the construct's architecture and porous interconnectivity. The challenge of 3D printing is the search for models that allow and facilitate the development of personalized constructs that meet the defect's optimal characteristics to be regenerated (Ref 21). Likewise, the characteristics mentioned above serve as an extracellular matrix (ECM) for colonization by stem cells, which have played a crucial role in regenerative engineering. Compared to other 3D printing techniques, the FDM technique has the lowest resolution; however, the printer used has a resolution of 0.2 μm, allowing the scaffold to build with homogeneous porosity.

In the dental area, mesenchymal stem cells derived from dental pulp (DPSC), which are easily accessible, express several transcription factors that are involved in the maintenance of self-renewal and present multipotency under defined culture conditions, differentiating in lineages osteogenic, adipogenic, chondrogenic, and neurogenic (Ref 22, 23). DPSCs are known to express markers related to bone tissue, similar to those in bone marrow-derived stem cells (BMSC). All anchor-dependent cells reside in an extracellular matrix (ECM); hence, a construct's primary goal is to create an environment that closely mimics natural ECM characteristics and allows cell adhesion and proliferation to function as they would do in vivo.

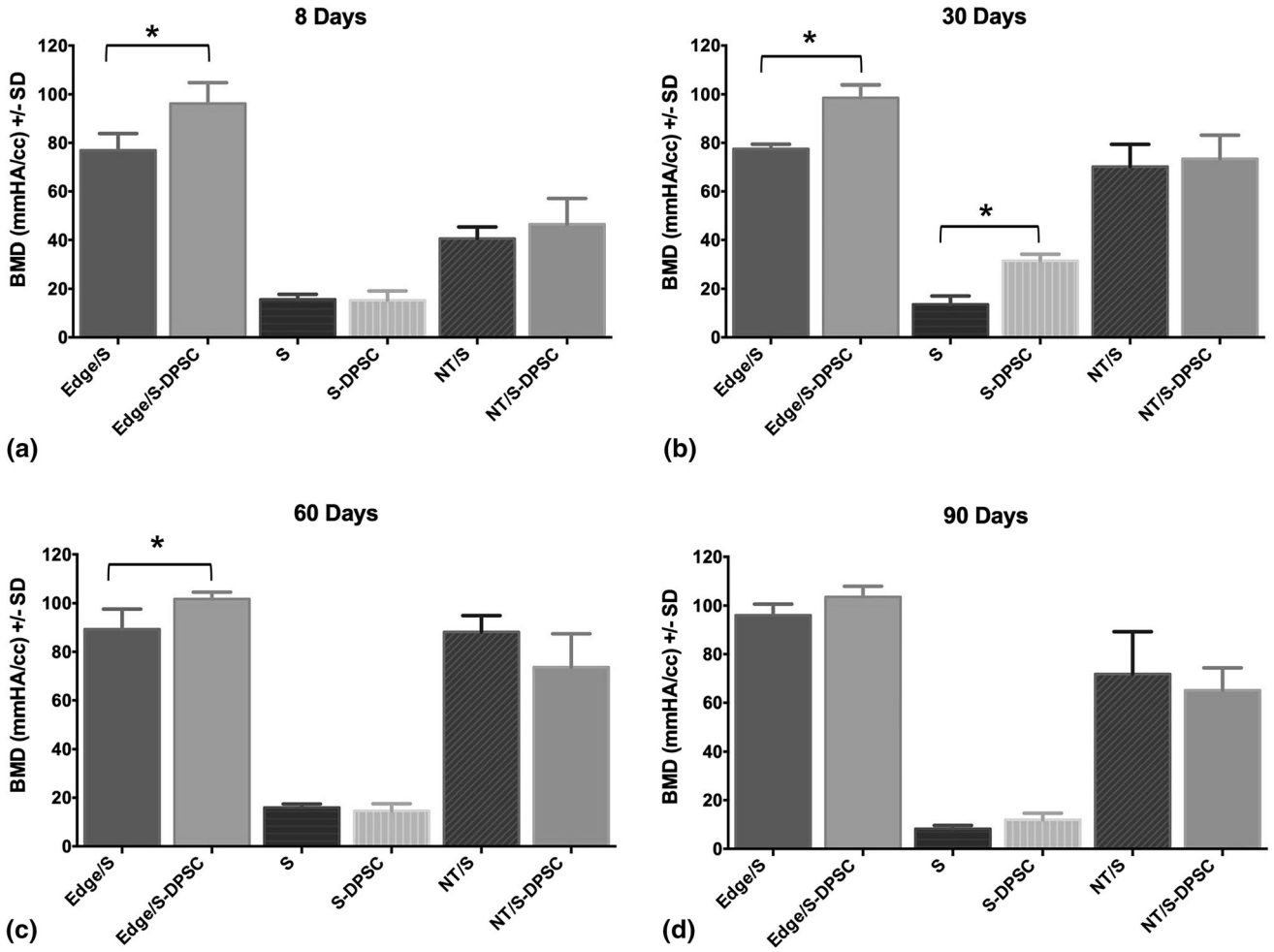

Fig. 4. Graphs where the BMD is compared by period of time of the different measurement zones. (a) 8 days, (b) 30 days, (c) 60 days, (d) 90 days

It should be noted that the characteristics of a scaffold affect the delivery of oxygen, nutrients, and the elimination of residues, one of the main characteristics being the porosity of the scaffold. For example, the pore size controls the tissue extension and the internal surface available for cell attachment. If the pores are too small, they are occluded by the cells, which prevents cell penetration, ECM production, and neovascularization in the scaffold's internal regions. On the contrary, with excessively large pores, the cells will not recognize the scaffolds specific micro-characteristics.

Most studies are suggesting that the pore size favors cell adhesion depending on the scaffold's material. Their study used PLA scaffolds and DPSC, with different pore sizes (Ref 15, 24). Cristian et al., in their study, demonstrated that a pore size from 100 to 200 µm promotes substantial bone growth, while a smaller pore size of 75-100 µm resulted in the formation of non-mineralized osteoid tissue (Ref 17). Moreover, Chung *et al.* mention that there is still no consensus on the optimal pore size necessary for cell growth and tissue formation (Ref 24).

Another important point concerning porosity is the functional gradualness reported by different authors (Ref 21, 25, 26). The term refers to constructs with graduated porosity, where the pore size decreases from the center to the periphery to mimic the natural structure of bone tissue, creating a favorable environment for cell growth and as a strategy to promote blood supply in the center of bone defects. Regarding the evaluation of the images by µCT, the experimental groups of this study showed a lesser novo tissue formation in the center of the bone defect compared to the edges; our results support the importance of gradualness in the novo tissue formation. Therefore, the synthesis of constructs with functional gradualness should be considered for tissue regeneration strategies.

Li *et al.,* when evaluating constructs printed in 3D with FDM technique functionalized with platelet-rich plasma (PRP), with a homogeneous porosity, examined the formation of bone matrix, in vitro, using DPSC seeded in the constructs. As in the present study, they evaluated bone formation in vivo, using critical size defects in calvaria of Wistar rats, and the results confirmed that the FDM technique permitted to control of the microarchitecture and the interconnection of the pores (200-300 µm) of the printed constructs. Their study confirmed that the DPSC cells adhere and proliferate in these constructs; besides, when performing the in vivo evaluation, there was mineralized novo tissue (Ref 27). The researchers suggested that the biological response is the result of the action of the presence of PRP. As for the present study, we verified through the in vitro WST-1 test that the pore size in these ranges was adequate and allow good biocompatibility and biological response. The constructs were manufactured with a homogeneous porosity,

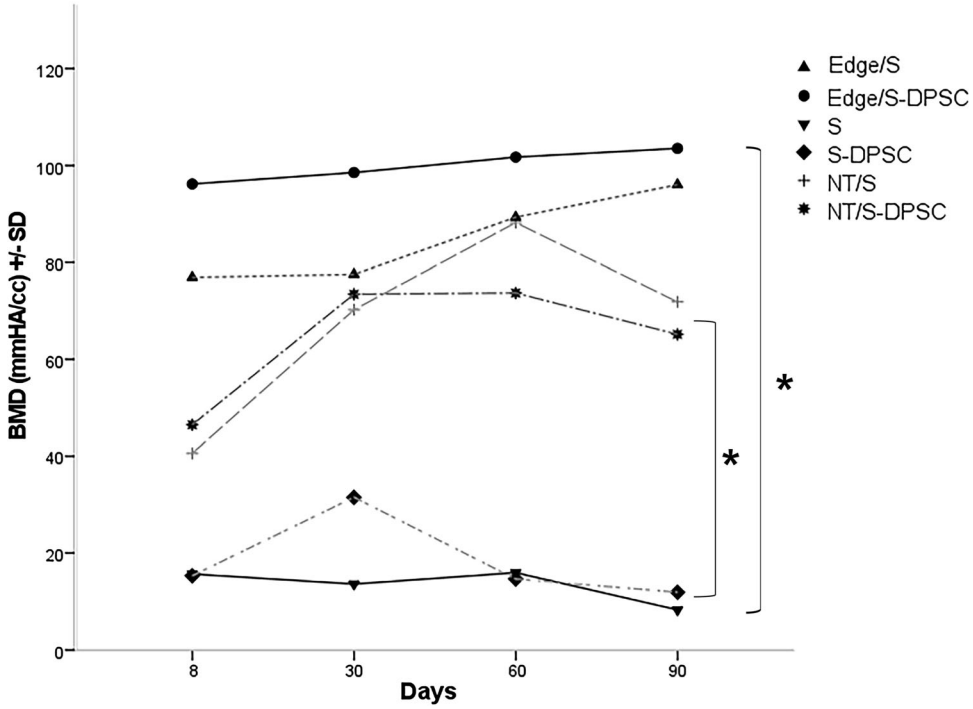

Fig. 5. Comparison of the BMD expressed in mmHA/cc of the groups on different days (8, 30, 60 and 90 days). Edge/S (3D-printed scaffold edge), Edge/S-DPSC (3D-printed scaffold edge with mesenchymal stem cells derived from dental pulp), S (3D-printed scaffold), S/DPSC (3D-printed scaffold with mesenchymal stem cells derived from dental pulp), NT/S (novo tissue in 3D-printed scaffold), NT/S-DPSC (novo tissue in 3D-printed scaffold with DPSC). The area that presented the highest BMD corresponds to the Edge/S-DPSC. It can be seen that where the measurement was made on the scaffolds, the one with the highest BMD corresponds to where DPSC was placed. Statistical significance is indicated by $*p < 0\ 05$

modifying a fundamental parameter in the Slic3r program, which is the filling density which was set at 85%, which allowed obtaining an approximate pore size of 214 μm, where the cells remained viable over the days, allowing the studies to be carried out in at in vivo bone model.

When performing the microtomographic image analysis, it was observed that the scaffold was adapted adequately to the size and shape of the bone defect. Moreover, the bone mineral density showed that the scaffold allowed the formation of novo mineralized tissue within the size critical defect, having similar results between the experimental group where the scaffold was implanted without the DPSC cells, compared to the group where the scaffold was implanted with the DPSC cells. On the other hands, up to 30 days, there were significant BMD differences in the adjacent bone between experimental groups. However, at day 90, there were no significant differences, which suggests that in the first days, the cells could have migrated toward the native bone area.

Considering another approach, it is suggested that the differentiation process of DPSC cells to bone lineage occurs in a long time compared to host mesenchymal stem cells because the bone lineage is not their priority cell destination for DPSC cells. However, the results also suggest that we would observe a more significant amount of novo tissue with a BMD similar to the native tissue in a longer study time.

According to the results, it was observed that at 90 days, the BMD in the novo tissue of both experimental groups decreased, possibly because the tissue that is being formed may be in the process of bone remodeling, which is a physiological process that takes place during bone regeneration. This process consists of the reabsorption of the clot, replaced by granulation tissue, and this stage is characterized by cellular mobilization and vascular growth mediated by angiopoietins and different vascular endothelial growth factors (VEGFs); also a considerable activity of macrophages and osteoclasts is responsible for removing and reabsorbing soft and hard tissue residues, for being gradually replaced by bone tissue (Ref 28). However, it is necessary to carry out complementary studies, such as histological and immunohistochemical analysis, to confirm that new tissue has the anatomical characteristics of bone tissue.

5. Conclusions

It is feasible to design custom constructs based on microtomographic images, which can be printed with a pore size suitable for DPSC. The 3D-printed constructs are considered biocompatible as they promoted good cell viability. The construct printed in 3D precisely to the size of the defects allowed no adverse reaction, confirming its biocompatibility. The 3D-printed construct could be considered osteoconductive, allowing novo tissue formation in the area of the defect. The novo tissue did not present a significant difference in BMD between both groups; however, it is not far from the BMD of the border, which makes it possible to postulate that in future approaches, these constructs could be seeded with stem cells, previously induced to bone lineage, enhancing the outcome of the regeneration process. It is important to mention that molecular studies are needed to verify a possible differentiation

process of the DPSC cells to the bone lineage and a histological evaluation of the novo tissue.

Acknowledgments

LPS want to thank to CONACYT scholarship support (No. 630955 with CVU: 853492) for her support in her Ph.D. studies in the Programa de Maestría y Doctorado en Ciencias Médicas, Odontológicas y de la Salud (PMDCMOS), UNAM.

Funding

The authors want to give their thanks for financial support from the DGAPA-UNAM: PAPIIT IN221020 and IN213821 projects and CONACYT through the particular program Fondo Sectorial de Investigación para la Educación A1S-9178.

Conflict of interest

There is no conflict of interest in this study.

References

1. R. Fairag, D.H. Rosenzweig, J.L. Ramirez-Garcialuna, M.H. Weber and L. Haglund, Three-Dimensional Printed Polylactic Acid Scaffolds Promote Bone-Like Matrix Deposition In Vitro, *ACS Appl. Mater. Interfaces*, 2019, **11**(17), p 15306–15315
2. Y. Fillingham and J. Jacobs, Bone Grafts and Their Substitutes, *CCJR Suppl. Bone Jt. J.*, 2016, **98-B**, p 6–9
3. D.L. Hoexter, Bone Regeneration Graft Materials, *J. Oral Implantol.*, 2002, **28**(6), p 3–7
4. P. Kumar, B. Vinitha and G. Fathima, Bone Grafts in Dentistry, *Dent. Sci.*, 2013, **5**, p 125–128
5. F. Guilak, D.L. Butler and S.A. Goldstein, Biomechanics and Mechanobiology in Functional Tissue Engineering, *J. Biomech.*, 2015, **47**(9), p 1933–1940
6. T. Liang, S. Mahalingam and M. Edirisinghe, Creating, "Hotels" for Cells by Electrospinning Honeycomb-Like Polymeric Structures, *Mater. Sci. Eng. C*, 2013, **33**(7), p 4384–4391
7. P. Bajaj, R.M. Schweller and A. Khademhosseini, 3D Biofabrication Strategies for Tissue Engineering and Regenerative Medicine, *Annu. Rev. Biomed. Eng.*, 2014, **16**, p 247–276
8. E. Castro-Aguirre, F. Iñiguez-franco, H. Samsudin, X. Fang and R. Auras, Poly (Lactic Acid)-Mass Production, Processing, Industrial Applications, and End of Life, *Adv. Drug Deliv. Rev.*, 2016, **107**, p 333–366
9. N. Nuti, C. Corallo, B.M.F. Chan and M. Ferrari, Multipotent Differentiation of Human Dental Pulp Stem Cells: A Literature Review, *Stem Cell Rev. Rep.*, 2016, **12**, p 9661–9669
10. M. Aurrekoetxea, P. Garcia-Gallastegui, I. Irastorza, J. Luzuriaga, V. Uribe-Etxebarria, F. Unda et al., Dental Pulp Stem Cells as a Multifaceted Tool for Bioengineering and the Regeneration of Craniomaxillofacial Tissues, *Front. Physiol.*, 2015, **6**, p 1–10
11. W. Zhang, X.F. Walboomers, K.T.H. Van, W.F. Daamen, Z. Bian and J.A. Jansen, The Performance of Human Dental Pulp Stem Cells on Different Three-Dimensional Scaffold Materials, *Biomed. Eng. Biomed. Technol.*, 2006, **27**, p 5658–5668
12. T. Yasui, Y. Mabuchi, H. Toriumi, T. Ebine, K. Niibe, D.D. Houlihan et al., Purified Human Dental Pulp Stem Cells Promote Osteogenic Regeneration, *J. Dent. Res.*, 2015, **95**(2), p 1–9
13. M.D.P. De la Rosa-Ruiz, M.A. Álvarez-Pérez, V.A. Cortés-Morales, A. Monroy-García, H. Mayani, G. Fragoso-González et al., Mesenchymal Stem/Stromal Cells Derived from Dental Tissues: A Comparative In Vitro Evaluation of Their Immunoregulatory Properties Against T cells, *Cells*, 2019, **8**(12), p 1491
14. F. Asa, G. Pagni, S.P. Pilipchuk, A.B. Giannì, W.V. Giannobile and G. Rasperini, 3D-Printed Scaffolds and Biomaterials: Review of Alveolar Bone Augmentation and Periodontal Regeneration Applications, *Int. J. Dent.*, 2016, **2016**, p 1–15
15. M. Ricardo, D. Oliveira, M.F. De, R. Bentini and F. Goncalves, The Performance of Bone Tissue Engineering Scaffolds in In Vivo Animal Models: A Systematic Review, *J. Biomater. Appl.*, 2016, **31**(5), p 625–636
16. G. Narayanan, V.N. Vernekar, E.L. Kuyinu and C.T. Laurencin, Poly (Lactic Acid)-Based Biomaterials for Orthopaedic Regenerative Engineering, *Adv. Drug Deliv. Rev.*, 2016, **107**, p 247–276
17. M. Cristian, M. Conde, F.F. Demarco, J.C. Alcazar, J.E. Nör and S. Beatriz, Influence of Poly-L-Lactic Acid Scaffolds Pore Size on the Proliferation and Differentiation of Dental Pulp Stem Cells, *Braz. Dent. J.*, 2015, **26**(2), p 93–98
18. M. Savaris, V. Santos and R.N. Brandalise, Influence of Different Sterilization Processes on the Properties of Commercial Poly (Lactic Acid), *Mater. Sci. Eng. C*, 2016, **69**, p 661–667
19. S. Cheruthazhekatt, Č Mirko, P. Slaví and J. Havel, Gas Plasmas and Plasma Modified Materials in Medicine, *J. Appl. Biomed.*, 2010, **8**(2), p 55–66
20. X. Qi, P. Pei and M. Zhu, Three-Dimensional Printing of Calcium Sulfate and Mesoporous Bioactive Glass Scaffolds for Improving Bone Regeneration In Vitro and In Vivo, *Sci. Rep.*, 2017, **7**, p 1–12
21. J. An, M. Teoh and R. Suntornnond, Design and 3D Printing of Scaffolds and Tissues, *Engineering*, 2015, **1**(2), p 261–268
22. W. Zhang, X.F. Walboomers, K.T.H. Van, W.F. Daamen, Z. Bian and J.A. Jansen, The Performance of Human Dental Pulp Stem Cells on Different Three-Dimensional Scaffold Materials, *Biomaterials*, 2006, **27**(33), p 5658–5668
23. F. Tatsuhiro, T. Seiko, T. Yusuke and T. Reiko, Dental Pulp Stem Cell-Derived, Scaffold-Free Constructs for Bone Regeneration, *Int. J. Mol. Sci.*, 2018, **19**, p 1–13
24. S. Chung and M.W. King, Design Concepts and Strategies for Tissue Engineering Scaffolds, *Biotechnol. Appl. Biochem.*, 2011, **58**(6), p 423–438
25. K. Leonga, C. Chuaa and N. Sudarmadjia, Engineering Functionally Graded Tissue Engineering Scaffolds, *J. Mech. Behav. Biomed. Mater.*, 2008, **1**, p 140–152
26. N. Yanga, Z. Quanc and D. Zhangd, Multi-morphology Transition Hybridization CAD Design of Minimal Surface Porous Structures for Use in Tissue Engineering, *Comput. Aided Des.*, 2014, **56**, p 11–21
27. J. Li, M. Chen and X. Wei, Evaluation of 3D-Printed Polycaprolactone Scaffolds Coated with Freeze-Dried Platelet-Rich Plasma for Bone Regeneration, *Materials*, 2017, **10**(7), p 1–16
28. W. Xiao, Y. Wang, S. Pacios, S. Li and D.T. Graves, Cellular and Molecular Aspects of Bone Remodeling, *Front. Oral Biol.*, 2015, **18**, p 9–16